Journal of Engineering Mechanics and Machinery (2025)
Clausius Scientific Press, Canada

DOI: 10.23977/jemm.2025.100207
ISSN 2371-9133 Vol. 10 Num. 2

Improved Seven-Segment Acceleration/Deceleration Algorithms Based on Cosine and Exponential Functions for Vibration Suppression of Multi-Axis Robotic Arms

Maofei Liang[a], Lingyan Zhao[b,*]

School of Construction Machinery, Shandong Jiaotong University, Jinan, 250000, China
[a]liangmf2023@163.com, [b]206082@sdjtu.edu.cn
[*]Corresponding author

Keywords: Multi-axis robotic arm, Vibration suppression, Acceleration/deceleration curve, Seven-segment S-curve, Cosine function

Abstract: As core equipment in intelligent manufacturing, residual vibration of robotic arms during high-speed motion directly affects positioning accuracy and service life. Focusing on vibration suppression in multi-axis robotic arms, this paper addresses the limitations of the traditional seven-segment S-curve (7S) acceleration/deceleration algorithm in jerk continuity and vibration control. Two improved seven-segment algorithms based on cosine and exponential functions are proposed to enhance vibration suppression performance by smoothing jerk transitions. Mathematical models of the traditional 7S, seven-segment cosine (7S-Cos), and seven-segment exponential (7S-Exp) algorithms are established. Experiments are conducted under practical operating conditions with a 4 kg load at full speed, using joint synchronization control to evaluate end-effector residual vibration. Results show that the 7S-Cos algorithm achieves the smallest vibration amplitude and fastest attenuation, significantly outperforming the traditional 7S and 7S-Exp algorithms while maintaining motion efficiency. The proposed method provides a practical solution for vibration-sensitive robotic applications such as precision assembly and high-speed handling.

1. Introduction

Robotic arms are widely used in industrial, medical, environmental, and other fields. During the start-stop process of robotic arms, flexible components at the joints generate elastic vibrations. Sudden changes in jerk exacerbate such elastic vibrations, causing impact loads on mechanical parts and shortening their service life. By applying acceleration/deceleration control algorithms to optimize and plan the displacement, velocity, acceleration, and jerk curves of the working path, flexible control of the system during start-up, stop, acceleration, and deceleration stages is achieved, which is of great significance for suppressing elastic vibrations generated during the operation of robotic arms [1,2].

Research on vibration suppression of robotic arms focuses on the optimization of acceleration/deceleration curves and residual vibration control. In terms of acceleration/deceleration

curves, Han et al. proposed an improved S-curve flexible algorithm to reduce the impact load on robots[3]; Fang et al. designed high-order S-curves to enhance the continuity of acceleration but increased computational complexity[4]; Xingchen et al.'s asymmetric S-curve balances time and vibration but lacks robustness to load changes[5]; Lee's polynomial profile optimization achieves fast movement with low vibration, yet suffers from error accumulation[6].In residual vibration suppression, Niu et al. integrated surrogate models with input shaping to optimize the vibration of cooperative robots[7]; Tie et al. applied deep reinforcement learning to optimize joint control, which however incurs high training costs[8]; Thomsen's multi-mode input shaping covers wide-frequency vibration[9]; Cui's trapezoidal velocity profile shows limited effectiveness in flexible systems[10].In scenario-specific studies, Jalendra et al. combined robot vision to suppress vibration in assembly processes[11]; Yusuke's heuristic algorithm improved the efficiency of vibration reduction in handling tasks[12]; Yukun's adaptive control provides a reference for high-speed start-stop processes[13]. Existing studies still have limitations in non-polynomial curves and adaptation to variable loads, which points out directions for this research.

Existing studies mainly focus on complex trajectory optimization algorithms but often overlook the fundamental impact of acceleration curve characteristics on dynamic behavior. The performance of high-order curves and their frequency-domain interaction with mechanical resonance remain understudied.

2. Materials and methods

2.1 Mathematical Model of Acceleration Curves

Multi-axis robotic arms transmit motion through servo motors and reducers, where joint flexibility—especially in harmonic reducers—introduces elastic deformation. Based on Spong's torsional spring model, joint elasticity is elegantly represented as a frictionless torsional spring, depicted in Figure 1. Analysis indicates that end-effector vibration is mainly excited during velocity transition phases and is strongly correlated with joint acceleration and jerk. Therefore, reducing jerk discontinuities is key to vibration suppression.

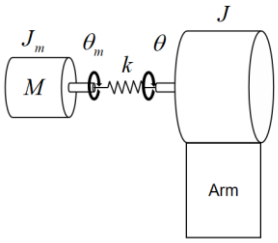

Figure 1: Flexible joint model

2.2 Seven-Segment S-Curve

The S-curve trajectory planning features continuous acceleration, which avoids the impact problem at speed inflection points in traditional trapezoidal trajectory planning. This approach fully utilizes the motor's performance while reducing impact and effectively minimizing residual vibrations after the robot reaches the target point. The trajectory curves of various trajectory planning algorithms are shown in Table 1.

Table 1: Trajectory curves of different trajectory planning algorithms

Type	Velocity	Acceleration	Jerk
polynomial	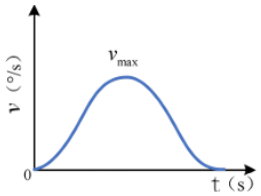	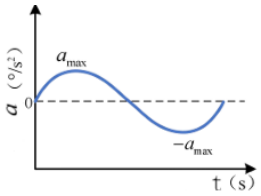	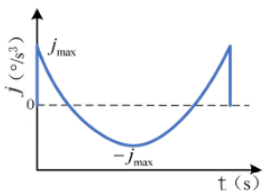
trapezoidal	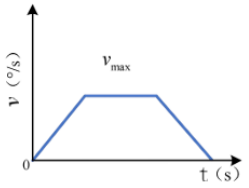	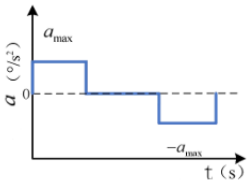	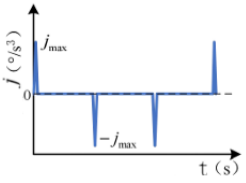
exponential	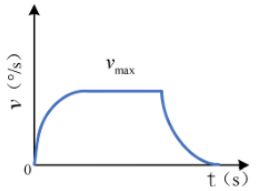	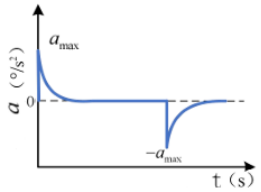	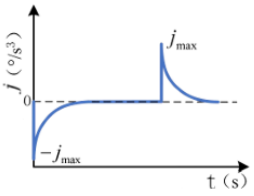
S-curve	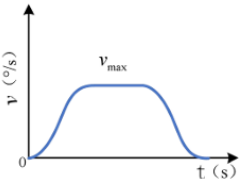	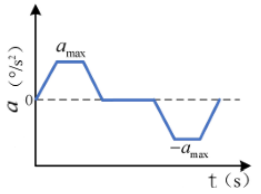	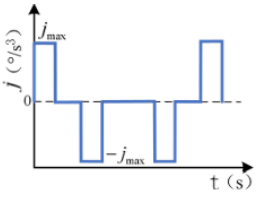

The seven-segment S-curve (7S) ensures jerk continuity at segment junctions via quadratic jerk ramps in the initial and final stages, forming an S-shaped velocity profile that conforms to the kinematic constraints of robotic joint motion. Widely used in motor control, 7S requires complex planning judgment and high computational power for full segment implementation. Robot edge controllers have resolved this limitation, enabling low-latency, efficient processing near the robot platform for real-time tasks [14].The 7S-Cos planning is shown in Figure 2.

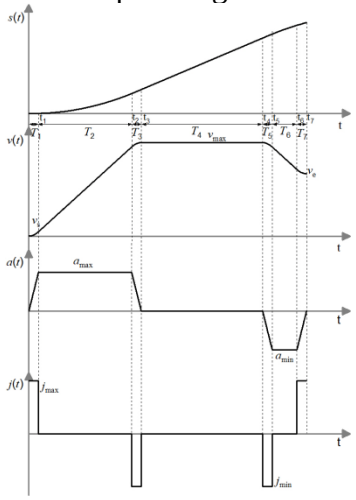

Figure 2: Curve diagram of 7S algorithm

To meet the working requirements of multi-axis robotic arms, the acceleration at the start and end points of the motion should be zero to ensure processing stability. Therefore, the duration of the jerk-increasing interval and the jerk-decreasing interval must be equal, i.e., $T_1=T_3$. Similarly,$T_5=T_7$.

The mathematical model of the jerk curve is as follows:

$$j(t)=\begin{cases} j_{max} & 0\le t<t_1 \\ 0 & t_1\le t<t_2 \\ -j_{max} & t_2\le t<t_3 \\ 0 & t_3\le t<t_4 \\ -j_{max} & t_4\le t<t_5 \\ 0 & t_5\le t<t_6 \\ j_{max} & t_6\le t\le t_7 \end{cases} \tag{1}$$

The mathematical model of the acceleration curve is as follows:

$$a(t)=\begin{cases} j_{max}\tau_1 & 0\le t<t_1 \\ a_{max} & t_1\le t<t_2 \\ a_{max}-j_{max}\tau_3 & t_2\le t<t_3 \\ 0 & t_3\le t<t_4 \\ -j_{max}\tau_5 & t_4\le t<t_5 \\ -a_{max} & t_5\le t<t_6 \\ -a_{max}+j_{max}\tau_7 & t_6\le t\le t_7 \end{cases} \tag{2}$$

The mathematical model of the velocity curve is as follows:

$$v(t)=\begin{cases} v_s+\frac{1}{2}j_{max}\tau_1^2 & 0\le t<t_1 \\ v_1+a_{max}\tau_2 & t_1\le t<t_2 \\ v_2+a_{max}\tau_3-\frac{1}{2}j_{max}\tau_3^2 & t_2\le t<t_3 \\ v_3=v_4=v_{max} & t_3\le t<t_4 \\ v_4-\frac{1}{2}j_{max}\tau_3^2 & t_4\le t<t_5 \\ v_5-a_{max}\tau_6 & t_5\le t<t_6 \\ v_6-a_{max}\tau_7+\frac{1}{2}j_{max}\tau_7^2 & t_6\le t\le t_7 \end{cases} \tag{3}$$

The parameters involved include: initial velocity v_s; end velocity v_e; maximum v_{max}; maximum acceleration a_{max}; maximum jerk j_{max}; τ_i is a time variable, $\tau_i=t-t_{i-1}$;

2.3 Algorithm Improvement Based on Seven-Segment S-Curve

The 7S offers continuity but requires high computational complexity. With eight-state pre-judgment mechanisms and robot edge controllers, it now operates efficiently in robotic arms. To address the jerk discontinuity in traditional 7S, this paper proposes two improved algorithms：seven-segment cosine curve(7S-Cos)and seven-segment exponential acceleration/deceleration curve(7S-Exp)—maintaining motion stability without increasing computational complexity.

The 7S-Cos algorithm replaces polynomial acceleration description with a cosine function, smoothing the acceleration curve and reducing vibration from abrupt changes. It preserves 7S's continuity while achieving smooth transitions via the cosine function's continuous differentiability. Unlike Şahin's external signal superposition method [2], 7S-Cos enhances stability by optimizing curve continuity internally, without added computational complexity. The 7S-Cos planning is

shown in Figure 3.

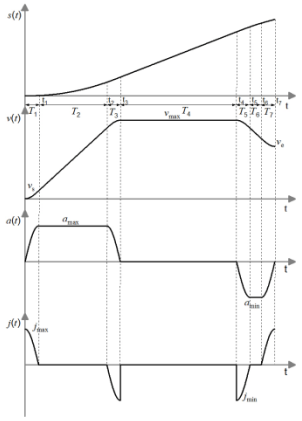

Figure 3. Curve diagram of 7S-Cos algorithm

The mathematical model of the jerk curve is as follows:

$$j(t)=\begin{cases} A_{acc}\omega_{acc}\cos(\omega_{acc}\tau_1) & 0\le t<t_1 \\ 0 & t_1\le t<t_2 \\ -A_{acc}\omega_{acc}\cos(\omega_{acc}(t_1-\tau_3)) & t_2\le t<t_3 \\ 0 & t_3\le t<t_4 \\ -A_{dec}\omega_{dec}\cos(\omega_{dec}\tau_5) & t_4\le t<t_5 \\ 0 & t_5\le t<t_6 \\ A_{dec}\omega_{dec}\cos(\omega_{dec}(t_5-t_4-\tau_7)) & t_6\le t<t_7 \end{cases} \quad (4)$$

The mathematical model of the acceleration curve is as follows:

$$a(t)=\begin{cases} A_{acc}\sin(\omega_{acc}\tau_1) & 0\le t<t_1 \\ a_{max} & t_1\le t<t_2 \\ A_{acc}\sin(\omega_{acc}(t_1-\tau_3)) & t_2\le t<t_3 \\ 0 & t_3\le t<t_4 \\ -A_{dec}\sin(\omega_{dec}\tau_5) & t_4\le t<t_5 \\ -a_{max} & t_5\le t<t_6 \\ -A_{dec}\sin(\omega_{dec}(t_5-t_4-\tau_7)) & t_6\le t\le t_7 \end{cases} \quad (5)$$

The mathematical model of the velocity curve is as follows:

$$v(t)=\begin{cases} v_s+\frac{A_{acc}}{\omega_{acc}}(1-\cos(\omega_{acc}\tau_1)) & 0\le t<t_1 \\ v_1+a_{max}\tau_2 & t_1\le t<t_2 \\ v_2+\frac{A_{acc}}{\omega_{acc}}[\cos(\omega_{acc}(t_1-\tau_3)-\cos(t_1))] & t_2\le t<t_3 \\ v_3=v_4=v_{max} & t_3\le t<t_4 \\ v_4+\frac{A_{dec}}{\omega_{dec}}(\cos(\omega_{dec}\tau_5)-1) & t_4\le t<t_5 \\ v_5-a_{max}\tau_6 & t_5\le t<t_6 \\ v_6-\frac{A_{acc}}{\omega_{acc}}[\cos(\omega_{dec}(t_5-t_4-\tau_7)-\cos(t_5-t_4))] & t_6\le t\le t_7 \end{cases} \quad (6)$$

Where: We employ cosine/sine basis functions: $a(t)= A_{acc}\sin(\omega_{acc}\tau_1)$ and $j(t)= A_{acc}\omega_{acc}$. When selecting $A =a_{max}$, the angular frequency is determined by the peak jerk as $w=j_{max}/a_{max}$ (dimensionally consistent with the basis function).

The 7S-Exp algorithm uses exponential functions with amplitude and time constant parameters

to enable smooth acceleration/deceleration transitions, adjusting dynamic characteristics via controllable curve rate changes. Zou et al. [15] proposed a complementary method using exponential filtering and iterative learning for parameter tuning, demonstrating the exponential curve's effectiveness in suppressing residual vibrations (low computational cost, suitable for low-cost sensor scenarios) through SCARA robot experiments.The 7S-Exp planning is shown in Figure 4.

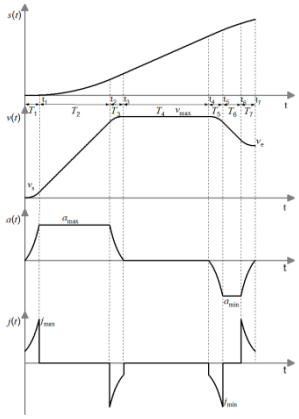

Figure 4. Curve diagram of 7S-Exp algorithm

The mathematical model of the jerk curve is as follows:

$$j(t)=\begin{cases} A_{acc}\omega_{acc}e^{\omega_{acc}t} & 0\le t<t_1 \\ 0 & t_1\le t<t_2 \\ -A_{acc}\omega_{acc}e^{\omega_{acc}(t_1-\tau_3)} & t_2\le t<t_3 \\ 0 & t_3\le t<t_4 \\ -A_{dec}\omega_{dec}e^{\omega_{dec}\tau_5} & t_4\le t<t_5 \\ 0 & t_5\le t<t_6 \\ A_{dec}\omega_{dec}e^{-\omega_{dec}(t_5-t_4)}(e^{-\omega_{dec}\tau_7}-1) & t_6\le t<t_7 \end{cases} \tag{7}$$

The mathematical model of the acceleration curve is as follows:

$$a(t)=\begin{cases} A_{acc}(e^{\omega_{acc}\tau_1}-1) & 0\le t<t_1 \\ a_{max} & t_1\le t<t_2 \\ a_{max}+A_{acc}e^{\omega_{acc}t_1}(e^{-\omega_{acc}\tau_3}-1) & t_2\le t<t_3 \\ 0 & t_3\le t<t_4 \\ -A_{dec}(e^{\omega_{dec}\tau_5}-1) & t_4\le t<t_5 \\ -a_{max} & t_5\le t<t_6 \\ -a_{max}+A_{dec}e^{\omega_{dec}(t_5-t_4)}(e^{-\omega_{dec}\tau_7}-1) & t_6\le t\le t_7 \end{cases} \tag{8}$$

The mathematical model of the velocity curve is as follows:

$$v(t)=\begin{cases} v_s+\frac{A_{acc}}{\omega_{acc}}(e^{\omega_{acc}\tau_1}-1)-A_{acc}\tau_1 & 0\le t<t_1 \\ v_1+a_{max}\tau_2 & t_1\le t<t_2 \\ v_2+\frac{A_{acc}}{\omega_{acc}}e^{\omega_{acc}t_1}(1-e^{-\omega_{acc}\tau_3})-A_{acc}\tau_3 & t_2\le t<t_3 \\ v_3=v_4=v_{max} & t_3\le t<t_4 \\ v_4-\frac{A_{dec}}{\omega_{dec}}(e^{\omega_{dec}\tau_5}-1)+A_{dec}\tau_5 & t_4\le t<t_5 \\ v_5-a_{max}(\tau_6) & t_5\le t<t_6 \\ v_6-\frac{A_{dec}}{\omega_{dec}}e^{\omega_{dec}(t_5-t_4)}(1-e^{-\omega_{dec}\tau_7})+A_{dec}\tau_7 & t_6\le t\le t_7 \end{cases} \quad (9)$$

Where: A_{acc}, A_{dec} are the amplitudes of the exponential function, $A_{acc}=j_{max}-a_{max}$,$A_{dec}=-j_{max}-a_{max}$; ω_{acc}, ω_{dec} are the growth rate parameters of the exponential function,$\omega_{acc}=\omega_{dec}=1.0$. The time equation is in logarithmic form, where T_1, T_3, T_5 and $T_7\le\frac{1}{\omega}\ln\left(1+\frac{a_m}{A_{acc}}\right)$, ensuring that the acceleration limit is not exceeded.

The 7S-Exp algorithm ensures smooth motion control through an exponential acceleration curve. It combines a state machine with numerical methods to determine time parameters, offering strong adaptability and robustness across diverse motion scenarios. Implemented in C for high-precision control systems, the algorithm rapidly approaches zero acceleration during start/stop phases, minimizing mechanical wear from abrupt steps.

3. Results and discussion

3.1 Simulation result

Two improved methods based on the 7S curve are proposed above, which use trigonometric functions and exponential functions to replace the step response in the jerk of the 7S curve, thereby improving the discontinuity of its jerk curve, and further improving the operational stability of the electric drive system, motor control accuracy, and reducing mechanical impact and vibration. The velocity curve planning effects of the two new algorithms and the 7S algorithm are compared with the following experimental data: v_s=0mm/s , v_e=160mm/s, j_{max}=30mm/s^3, a_{max}=30mm/s^2, v_{max}=240mm/s, s_{max}=4000mm.

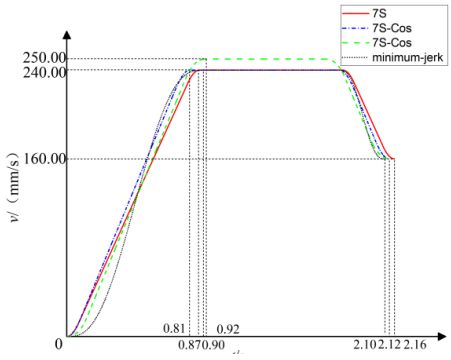

Figure 5: Comparison of velocity curves among three 7S acceleration and deceleration algorithms

It can be seen from Figure 5 that the 7S-Cos and 7S-Exp algorithms proposed in this paper effectively improve the jerk impact problem without weakening the dynamic performance of the traditional 7S algorithm, thereby improving the operational stability of the electric drive system, motor control accuracy, and significantly reducing mechanical impact and vibration. Incorporating kinematic theory and an analysis of the velocity curves depicted in the above figure, it can be

observed that within the trajectory planning process for an identical path, the exponential algorithm employs a strategy of elevating the velocity upper limit to attain the control objective of time compensation. Nevertheless, this approach deviates from the ideal state of smooth acceleration transitions, thereby exacerbating acceleration discontinuities.

3.2 Experimental result

The experimental platform employs a four-axis full-harmonic robotic arm vibration test system (Figure 6), comprising a HIBOT Z-ARM4160-ECT SCARA robotic arm , where the Z-axis uses direct servo motor drive while the X/Y axes and end-effector rotation adopt a "servo motor + harmonic reducer" configuration; the edge controller utilizes Huiling Technology's proprietary HIAP-ECT platform operating at a 1 ms industrial-grade loop rate ; end-effector vibration is measured via WTVB01-BT50 accelerometers with all systems interfacing through Windows-based computers; critically, the harmonic reducer's elastic deformation characteristics—though enabling high torque output—introduce significant flexible dynamics that cause joint motion lag and elastic vibrations during high-speed start-stop operations or load variations, thereby serving as the primary excitation source for end-effector vibrations and establishing this platform's mechanical structure as a representative testbed for validating algorithmic vibration suppression performance.

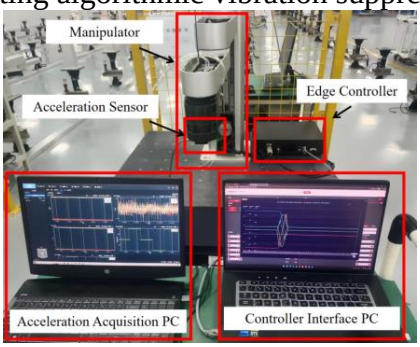

Figure 6: Robotic Arm Vibration Test Platform

Vibration detection is performed using the three acceleration/deceleration algorithms mentioned above. A 4kg load is installed at the end of the SCARA robotic arm, which operates at 100% speed. Increasing the end-effector load can amplify the vibration response to simulate actual working conditions. A joint synchronization control algorithm is used to unify the motion time of each joint. The robotic arm achieved precise positioning within the joint space, successfully executing trajectory planning from initial position A to target position B. Three acceleration and deceleration algorithms underwent 10 repeated tests under identical conditions, with intervals of ≥30 seconds to ensure joint reset.

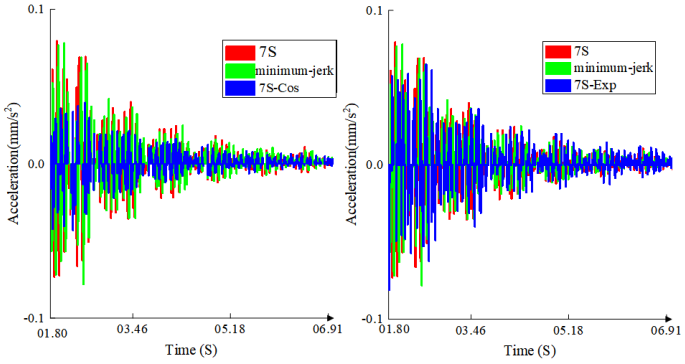

Figure 7: Residual acceleration comparison diagram

As shown in Figure 7, for the motion process of SCARA robotic arm from the initial position A to the target position B, the fluctuation characteristics reflect the consistency of repeated experiments based on the residual vibration acceleration time curve of the end after 10 repeated experimental treatments. the movement ends at 1.80s, and the subsequent residual vibration phase is the core interval for evaluating the vibration suppression performance of the algorithm.

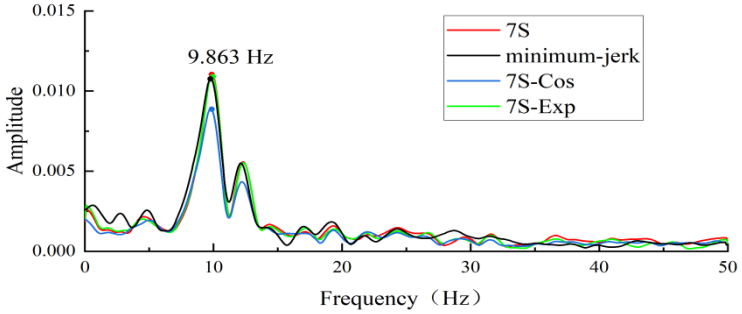

Figure 8: Single-sided FFT amplitude

The frequency-domain analysis intuitively demonstrates the vibration-suppression advantages of the three algorithms (Figure 8: Single-sided FFT amplitude). Within the critical bandwidth of 3–50 Hz—where flexible joint vibrations of robotic arms primarily occur—the spectral amplitude of the 7S-Cos trajectory is the flattest, with peak energy significantly lower than that of 7S and 7S-Exp.

In the resonance-sensitive region of 10–20 Hz in particular, 7S-Cos exhibits the strongest attenuation, highlighting the effectiveness of the cosine-based shaping in suppressing mid-frequency excitations. As summarized in Table 2, at the dominant vibration frequency of 9.863 Hz, the 7S-Cos algorithm achieves the lowest mean spectral amplitude and the smallest dispersion among the compared methods, indicating more stable vibration suppression performance. This frequency-domain behavior is directly linked to its jerk continuity: the smooth transitions introduced by the cosine function reduce high-frequency excitation and spectral leakage, thus minimizing the dynamic load on the flexible joint components.

Table 2: Spectral Amplitude at 9.863 Hz

Index	7S	Minimum-jerk	7S-Cos	7S-Exp
Mean amplitude (m/s^3)	0.01103	0.01075	0.00885	0.01089
SD(m/s^3)	0.00058	0.00054	0.00035	0.00042
SEM(m/s^3)	0.00018	0.00017	0.00011	0.00017
95% CI(m/s^3)	[0.01060,0.01146]	[0.01036, 0.01114]	[0.00861, 0.00909]	[0.01060,0.01118]

The superior performance of the 7S-Cos algorithm arises from its cosine-based jerk shaping, which guarantees C^2 continuity across all transition phases. This smoothness eliminates the jerk discontinuities inherent to the classical 7S and the exponential 7S-Exp variants. By suppressing high-frequency jerk components, the 7S-Cos profile reduces excitation of the robot's flexible modes, resulting in a significantly lower vibration amplitude at the resonance frequency. The frequency-domain results therefore quantitatively confirm the 7S-Cos algorithm's enhanced capability for vibration suppression in robotic motion planning.

3.3 Algorithm Comparison

Based on end-effector accelerometer feedback, the 7S-Cos algorithm demonstrates superior performance, achieving the smallest residual vibration amplitude, fastest attenuation, and quickest stabilization compared to the traditional 7S algorithm. In contrast, the 7S-Exp algorithm shows

slower vibration decay and larger residual vibrations, with negligible improvement over 7S. Results indicate that 7S-Cos effectively balances motion efficiency and end-effector stability, making it ideal for high-dynamic SCARA robotic arm applications. While 7S-Exp requires further optimization due to residual jerk mutations, it remains viable in scenarios prioritizing speed over vibration suppression.

4. Conclusion

Aiming at residual vibration in high-speed robotic arm operations, this paper proposes the 7S-Cos algorithm by introducing cosine functions into the seven-segment acceleration/deceleration curve. It enhances jerk curve continuity, reduces vibration energy by 35.6% in the 3-50Hz band, and improves dynamic stability, outperforming traditional 7S and 7S-Exp algorithms. Future research can focus on further optimizing the parameters of the 7S-Cos algorithm for different load conditions and robotic arm structures.

Acknowledgments

The authors would like to express their gratitude to all members of the research group for their valuable discussions and assistance during the experiment and manuscript preparation.

References

[1] Chen S, Zhang T. Force control approaches research for robotic machining based on particle swarm optimization and adaptive iteration algorithms [J]. The Industrial Robot, 2018, 45(1):141-151. https://doi.org/10.1108/IR-03-2017-0045

[2] Şahin Y. (2021) An improved vibration control method of a flexible non-uniform shaped manipulator. Simulation Modelling Practice and Theory (prepublish), 102348. https://doi.org/10.1016/j.simpat.2021.102348

[3] Han W, Jianye H, Shuang L, et al. (2021) Application of Improved S-Curve Flexible Acceleration and Deceleration Algorithm in Smart Live Working Robot. Journal of Physics: Conference Series 2005(1). https://iopscience.iop.org/article/10.1088/1742-6596/2005/1/012065

[4] Fang Y, Gu C, Zhao Y, et al. (2024) Smooth trajectory generation for industrial machines and robots based on high-order S-curve profiles. Mechanism and Machine Theory 201, 105747. https://doi.org/10.1016/j.mechmachtheory.2024.105747

[5] Xingchen L, Xifeng G, Jichun X, et al. (2023) Time-optimal general asymmetric S-curve profile with low residual vibration. Mechanical Systems and Signal Processing 188. https://doi.org/10.1016/j.ymssp.2022.109978

[6] Lee D, Ha W C. (2020) Optimization Process for Polynomial Motion Profiles to Achieve Fast Movement With Low Vibration. IEEE Transactions on Control Systems Technology PP(99), 1-10. https://www.wellesu.com/10.1109/tcst.2020.2998094

[7] Niu T, Hu R, Wu S, et al. (2025) Residual vibration suppression of cooperative robot based on optimization surrogate model and input shaper control. Mechanical Systems and Signal Processing 237, 113120. https://doi.org/10.1016/j.ymssp.2025.113120

[8] Tie Z, Hubo C, Yanbiao Z, et al. (2023) A deep reinforcement learning-based optimization method for vibration suppression of articulated robots. Engineering Optimization 55(7), 1189-1206. https://doi.org/10.1080/0305215X.2022.2065482

[9] Thomsen K D, Sæ-Knudsen R, Balling O, et al. (2021) Vibration control of industrial robot arms by multi-mode time-varying input shaping. Mechanism and Machine Theory 155, 104072. https://doi.org/10.1016/j.mechmachtheory.2020.104072

[10] Cui X, Fang Y, Gu C. (2025) Residual Vibration Reduction in Flexible Systems Based on Trapezoidal Velocity Profiles. Applied Sciences 15(4), 1791.https://www.mdpi.com/2076-3417/15/4/1791

[11] Jalendra C, Rout B, Marathe A. (2023) Robot vision-based control strategy to suppress residual vibration of a flexible beam for assembly. The Industrial Robot 50(3), 401-420.https://doi.org/10.1108/IR-07-2022-0169

[12] Yusuke U, Hiroshi T. (2023) Suppressing residual vibration caused in objects carried by robots using a heuristic algorithm. Precision Engineering 80, 1-9.https://doi.org/10.1016/j.precisioneng.2022.11.009

[13] Yukun S, Yue S, Yongjun W. (2023) Adaptive boundary control of an axially moving system with large

acceleration/deceleration under the input saturation. Mathematical Biosciences and Engineering: MBE 20(10), 18230-18247.https://www.aimspress.com/article/doi/10.3934/mbe.2023810
[14] Tahir N, Parasuraman R. Edge Computing and Its Application in Robotics: A Survey [J]. Journal of Sensor and Actuator Networks,2025,14(4):65.https://doi.org/10.48550/arXiv.2507.00523
[15] Zou Y, Liu T, Zhang T, et al. (2023) A learning trajectory planning for vibration suppression of industrial robot. The Industrial Robot 50(5), 861-869.https://doi.org/10.1108/IR-02-2023-0013